MIMO-OFDM-Based Wireless-Powered Relaying Communication With an Energy Recycling Interface

Ali Arshad Nasir, *Member, IEEE*, Hoang Duong Tuan, Trung Q. Duong, *Senior Member, IEEE*, and H. Vincent Poor, *Fellow, IEEE*

***Abstract*— This paper considers wireless-powered relaying multiple-input-multiple-output (MIMO) communication, where all four nodes (information source, energy source, relay, and destination) are equipped with multiple antennas. Orthogonal frequency division multiplexing (OFDM) is applied for information processing to compensate the frequency selectivity of communication channels between the information source and the relay and between the relay and the destination as these nodes are assumed to be located far apart from each. The relay is equipped with a full-duplexing interface for harvesting energy not only from the wireless transmission of the dedicated energy source but also from its own transmission while relaying the source information to the destination. The problem of designing the optimal power allocation over OFDM subcarriers and transmit antennas to maximize the overall spectral efficiency is addressed. Due to a very large number of subcarriers, this design problem poses a large-scale nonconvex optimization problem involving a few thousand variables of power allocation, which is very computationally challenging. A novel path-following algorithm is proposed for computation. Based on the developed *closed-form* calculation of linear computational complexity at each iteration, the proposed algorithm rapidly converges to an optimal solution. Compared to the best existing solvers, the computational complexity of the proposed algorithm is reduced at least 10^5 times, making it very efficient and practical for online computation while existing solvers are ineffective. Numerical results for a practical simulation setting show promising results by achieving high spectral efficiency.**

***Index Terms*— Wireless-powered network, full-duplex interface, energy recycle, MIMO-OFDM relaying communication, spectral efficiency, power allocation, large-scale nonconvex optimization, online computation.**

Manuscript received May 10, 2019; revised August 2, 2019 and September 25, 2019; accepted November 1, 2019. Date of publication November 11, 2019; date of current version February 14, 2020. This work was supported in part by the KFUPM Research Project #SB171005, in part by Institute for Computational Science and Technology, Hochiminh City, Vietnam, in part by the Australian Research Council's Discovery Projects under Project DP190102501, in part by a U.K. Royal Academy of Engineering Research Fellowship under Grant RF1415\14\22, and in part by the U.S. National Science Foundation under Grants CCF-0939370, CCF-1513915 and CCF-1908308. The associate editor coordinating the review of this article and approving it for publication was Z. Zhang. *(Corresponding author: Trung Q. Duong.)*

A. A. Nasir is with the Department of Electrical Engineering, King Fahd University of Petroleum and Minerals (KFUPM), Dhahran 31261, Saudi Arabia (e-mail: anasir@kfupm.edu.sa).

H. D. Tuan is with the School of Electrical and Data Engineering, University of Technology Sydney, Ultimo, NSW 2007, Australia (e-mail: tuan.hoang@uts.edu.au).

T. Q. Duong is with the School of Electronics, Electrical Engineering and Computer Science, Queen's University Belfast, Belfast BT7 1NN, U.K. (e-mail: trung.q.duong@qub.ac.uk).

H. V. Poor is with the Department of Electrical Engineering, Princeton University, Princeton, NJ 08544 USA (e-mail: poor@princeton.edu).

Color versions of one or more of the figures in this article are available online at http://ieeexplore.ieee.org.

Digital Object Identifier 10.1109/TCOMM.2019.2952897

I. Introduction

A. Motivation and Literature Survey

FULL-DUPLEXING (FD) is an advanced fifth generation (5G) communication technology for signal transmission and reception at the same communication node, at the same time, and over the same frequency band [1], [2]. On the other hand, wireless power transfer is a promising solution which can assist in powering massive numbers of devices in Internet of Things (IoT) in 5G and future communication systems [3]. This is because battery replacement is a crucial issue for the massive number of wireless sensors in the IoT [4], [5]. Thus, FD and wireless power transfer technologies can provide a promising blend to improve the spectral efficiency and sensors' life-time for future communication systems.

An FD wireless-powered relay simultaneously splits the received signal for EH and information decoding (ID) [6]–[12]. Different communication settings, e.g., single-input-single-output (SISO) communication [6], SISO communication with multiple relays and relay selection [9], multiple-input-single-output (MISO) communication [7], [8], two-way relaying with multiple-antenna relay and FD source nodes [10], multiple-input multiple-output (MIMO) communication [11], [12], have been considered. However, the power-splitting approach is complicated and inefficient for practical implementation due to the requirement of a variable power-splitter design [13]. More importantly, the major issue in FD-based communication is the loop self-interference (SI) due to the co-location of transmit and receive antennas. With the current state-of-the-art technology of signal isolation and rejection, it is still not practical to mitigate the FD SI to a level worthy for simultaneous high uplink and downlink throughput [14]. Two-way relaying within one time-slot by an FD relay cannot be more efficient than that by a half-duplex relay in two time slots [15], [16]. However, such high-powered interference of the signal transmission to the signal reception by FD can open an opportunity for the simultaneous information transmission and energy-harvesting [17]. Indeed, unlike the information throughput, which is dependent on the signal-to-interference-plus-noise-ratio and thus suffers from the interference, the harvested energy is critically dependent on how strong the received signal power is, and hence, it can be enhanced by the interference as a complementary energy

source. Therefore, FD is natural for transmitting information while harvesting energy with self-energy recycling in wireless-powered networks [18]–[22]. In relaying communication, the information source sends the information signal to the relay in a first phase, and in a second phase, the energy source transfers the energy signal to the relay while the relay simultaneously harvests energy and forwards the information to the destination. Thus, an energy constrained relay can replenish its energy by harvesting energy from the signal composite of the source's energy signal and its own transmitted signal [19]. Using this protocol, different communication settings, e.g., SISO communication from the source-to-relay and MISO communication from the relay-to-destination [23], single-input-multiple-output (SIMO) communication from the source-to-relay and MISO communication from the relay-to-destination [24], [25], SISO communication over both links [26]–[29], MISO communication over both links [19], [30], [31], SISO communication with multiple relays and relay selection [32], MIMO communication from the source-to-relay and MISO link from the relay-to-destination [33], and MIMO communication over both links [20], have been considered.

One of the main issues of long range communication with MIMO setting is its channel frequency selectivity due to multipath propagation, which can be compensated by orthogonal frequency division multiplexing (OFDM) technology. By transforming the frequency selective channel into parallel frequency flat sub-channels, MIMO-OFDM provides the dominant air interface for broadband wireless communications [34], [35]. The communication range can be further extended by deploying cooperative relaying based communication to assist the transmission between the two distant ends. Considering relay-assisted networks, resource allocation in OFDM based communication with half-duplex (HD) relaying [36], [37] and FD relaying [15], [38] has been investigated. In addition, there are several recent studies which investigate EH in OFDM based systems too to address the needs of energy constrained nodes [39]–[41]. Wireless information and power transfer in HD OFDM relay networks is considered in [42]. However, as mentioned above, FD relaying in energy constrained network with the practical two-phase communication has a natural advantage (see [19], [20], [23]–[30], [32], [33] for non-OFDM systems). This is because during the second phase of communication, the energy constrained FD relay has the opportunity to harvest energy not only from the wireless energy signal from the source but also through the energy recycled from its own transmission.

B. Research Gap and Contribution

It must be realized that the physical conditions for wireless information and energy transfers are distinct. In fact, as EH is possible only when the power of the received energy signal passes a threshold that is very large compared to the power of the received information signal [17], [43], the energy transfer can be implemented only when the source is located very near to the relay. With the source node located near to the relay as in [24], [26], [27], [30], [32], the distances from the source to the relay and from the relay to the destination are not much different. The direct communication from the source to the destination is then preferred, and the energy transfer to the relay is superfluous.

Relaying communication is needed when the source node is located farther away from the relay as in [19], [42], but certainly the energy transfer from this node cannot be implemented because the received signal power will not pass the threshold for EH at the relay.

This paper considers a practical two-phase MIMO-OFDM communication system assisted by a wireless-powered FD relay. To avoid the aforementioned impractical assumptions, it proposes a dedicated *energy source* in the network, which is placed in a close vicinity of the relay node to transmit a wireless energy signal to the relay during the second communication phase. Thus, the relay harvests energy both from the recycled energy from its own transmission and from the wireless energy signal from the energy source. It is noteworthy that the dedicated energy source is definitely required for EH because the received signal power at the FD relay from its own transmission (loop SI) does not pass the threshold for EH at the relay. Under this practical setup with a dedicated energy source, the *information source* is located quite far from the destination, which transmits the information signal to the relay during the first communication phase. The key contributions of this work are as follows:

- This is the first paper to consider practical two-phase MIMO-OFDM communication assisted by a wireless-powered FD relay. The MIMO-OFDM relaying is needed to assist the communication between the information source and destination, which are located far apart from each other. The energy source is set to be placed sufficiently near to the relay to enable practical EH by the latter, which moreover uses FD to recycle the energy leaked from its signal transmission. The problem of designing the precoding and relaying matrices to maximize the overall spectral efficiency is formulated. Under MIMO-OFDM, the design of precoding and relaying matrices is simplified to that of power allocation over multiple subcarriers and transmit antennas.
- The optimization problem of power allocation is not only nonconvex but is large-scale due to a large number of subcarriers (up to thousands), making all the existing nonconvex solvers useless. This is the first paper to propose a path-following algorithm, which is practical for large-scale nonconvex optimization of thousands of variables (subcarriers). The algorithm is based on several innovative approximations for both concave and nonconcave functions, and for both convex and nonconvex sets, which enable the iterative optimization problem to admit the optimal solution in a closed-form. In particular, approximating a concave function by another concave function and a convex set by another convex set for a closed form of the optimal solution is a new idea in optimization.
- The proposed algorithm guarantees a computational solution, in about in one-tenth of a second, even in the presence of thousands of subcarriers, due to rapid convergence and linear computational complexity. The detailed

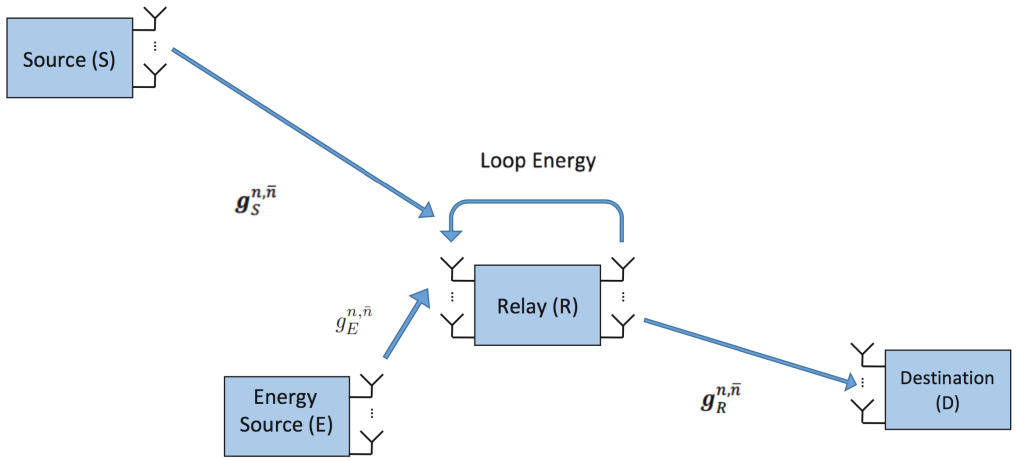

Fig. 1. Wireless-powered relaying with self-energy recycling.

computational complexity analysis clearly shows very substantial computational gain of the proposed algorithm compared to existing algorithms, which already struggle to work for small-scale systems with a few subcarriers due to their inherent high computational complexity. Particularly, comparing to the best existing solvers, the computational complexity of the proposed algorithm is reduced at least 10^5 times, making it quite efficient and practical for online computation. The provided numerical results with practical simulation settings show promising results by achieving high spectral efficiency.

C. Organization and Notation

Organization: The paper is organized as follows. After a brief description of the model, Section II presents the formulation of the rate maximization problem. Section III describes the proposed solution to the problem. Section IV evaluates the performance of our proposed algorithm by assuming a practical simulation setting. Finally, Section V concludes the paper.

Notation: Bold-face upper-case letters, e.g., $\mathbf{X}$ are used for matrices. Bold-faced lower-case letters, e.g., $\mathbf{x}$, are used for vectors and non-bold lower-case letters, e.g., x, are used for scalars. $[\mathbf{X}]_{a,b}$ represents the $(a,b)^{\text{th}}$ entry (a^{th} row, b^{th} column) of the matrix $\mathbf{X}$. The Hermitian transpose and normal transpose of the vector $\mathbf{x}$ are denoted by $\mathbf{x}^H$, and $\mathbf{x}^T$, respectively. $\mathbb{C}$ is the set of all complex numbers and $\mathbb{R}$ is the set for all real numbers. $\frac{\partial f(x)}{\partial x}$ is the derivative of the function $f(\cdot)$ with respect to its variable x. Finally, $\mathbb{E}(X)$ denotes the expectation of the random variable X.

II. System Model and Problem Formulation

Consider a cooperative communication system in which an energy constrained relay node (R) assists the communication between a source node (S) and a destination node (D). We assume that D is out-of-reach from S and there is no direct communication link between them. As shown in Fig. 1, a dedicated energy source (E) is placed in a close vicinity of the relay node to assist in fulfilling the energy requirements of the relay node. S, D, and E are equipped with N antennas but R is equipped with N transmit antennas and N receive antennas.[1]

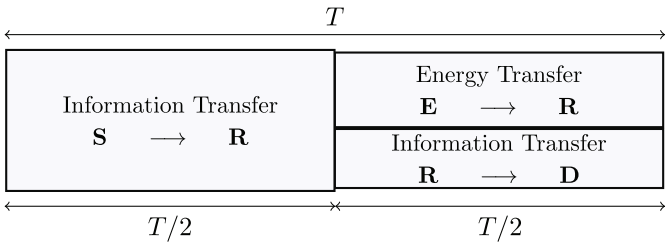

Fig. 2. Protocol for full-duplex wireless-powered relaying.

As shown in Fig. 2, the communication from S to D takes place in two-phases. During the first phase, S sends an information signal to R. During the second phase, E sends an energy signal to R and at the same time, R forwards the source information to D. Note that during the second stage, R harvests energy not only from the dedicated wireless energy signal from E but also from its own transmission. In other words, the self-interfering link at R enables the self-energy recycling.

Due to multipath propagation, the MIMO channel from S to R and from R to D is frequency selective. To combat such multipath channel distortion, multi-carrier modulation, i.e., OFDM is employed for transmitting the information-bearing signal from S to R in the first phase and also for forwarding it by R to D in the second phase. The channel between E and R is assumed frequency flat due to the short distance between them and thus the energy signal is transmitted by a single carrier.

Let the L-tap multipath channel from the antenna n at S to the antenna $\bar{n}$ at R be denoted by $\mathbf{g}_S^{n,\bar{n}} \in \mathbb{C}^L$ and that from the antenna n at R to the antenna $\bar{n}$ at D be denoted by $\mathbf{g}_R^{n,\bar{n}} \in \mathbb{C}^L$, $n, \bar{n} \in \{1, \ldots, N\}$. Due to the line-of-sight link between E and R, the channel between them can be modeled by a single-tap channel, which is denoted by

[1]Under general assumption of N_t transmit antennas and N_r receive antennas, N will refer to the number of spatially independent paths or the rank of the channel matrix, i.e., $N = \min(N_t, N_r)$.

$g_E^{n,\bar{n}} \in \mathbb{C}$. By incorporating the effect of large scale and small scale fading, the channel gain $g_E^{n,\bar{n}}$ is assumed to be Rician distributed, while all the channel taps of $\mathbf{g}_S^{n,\bar{n}}$ and $\mathbf{g}_R^{n,\bar{n}}$ are assumed to be Rayleigh distributed. It is also assumed that the full channel state information (CSI) is available by some high-performing channel estimation mechanism, and a central processing unit accesses that information to optimize resource allocation under perfect timing and carrier frequency synchronization. Particularly, using standard channel estimation techniques, the relay node can estimate the S-to-R channel $\mathbf{g}_S^{n,\bar{n}}$, and the E-to-R channel $g_E^{n,\bar{n}}$, and the destination node can estimate the R-to-D channel, $\mathbf{g}_R^{n,\bar{n}}$, which are sent to the central processing unit to solve the resource allocation problem. Note that the performance of the proposed resource allocation algorithm will be later analyzed under imperfect CSI in Section IV-B.

In the following the system model for information and energy processing is presented, which is followed by the problem formulation.

A. Information Processing

Using the fast Fourier transform (FFT), the received vector $\tilde{\mathbf{y}}_{R,k} \in \mathbb{C}^N$ at the relay on subcarrier $k \in \{1, 2, \ldots, K\}$ is given by

$$\tilde{\mathbf{y}}_{R,k} = \mathbf{H}_{S,k}\tilde{\mathbf{s}}_{ID,k} + \tilde{\mathbf{w}}_{R,k}, \tag{1}$$

where

- $\mathbf{H}_{S,k} \in \mathbb{C}^{N\times N}$ is the MIMO channel matrix between S and R on subcarrier k such that any element of $\mathbf{H}_{S,k}$, e.g., $(n, \bar{n})$th element, $[\mathbf{H}_{S,k}]_{n,\bar{n}}$, represents the sub-channel k between the transmit antenna n of S and the receive antenna $\bar{n}$ of R, i.e., we can obtain $[\mathbf{H}_{S,k}]_{n,\bar{n}}$, $k = \{1, \ldots, K\}$ by evaluating the K-point FFT of $\mathbf{g}_S^{n,\bar{n}}$,
- $\tilde{\mathbf{s}}_{ID,k} = \mathbf{\Psi}_k \mathbf{s}_{ID,k}$, $\mathbf{\Psi}_k \in \mathbb{C}^{N\times N}$ is the transmit precoding matrix on subcarrier k, $\mathbf{s}_{ID,k} \in \mathbb{C}^N$ is the modulated information data (ID) on subcarrier k,
- $\tilde{\mathbf{w}}_{R,k} \in \mathbb{C}^N$ is the additive zero-mean Gaussian noise with covariance $\boldsymbol{\mathcal{R}}_R = \sigma_R \mathbf{I}_N$, σ_R is the noise variance at each receive antenna and $\mathbf{I}_N$ is the $N \times N$ identity matrix.[2]

During the second phase, R amplifies the received signal vector on subcarrier k by a matrix $\mathbf{F}_k \in \mathbb{C}^{N\times N}$ and forwards the processed signal vector to D. The received vector $\tilde{\mathbf{y}}_{D,k} \in \mathbb{C}^N$, after FFT, on subcarrier $k \in \{1, 2, \ldots, K\}$ at the destination is given by

$$\tilde{\mathbf{y}}_{D,k} = \mathbf{H}_{R,k}\mathbf{F}_k \left(\mathbf{H}_{S,k}\tilde{\mathbf{s}}_{ID,k} + \tilde{\mathbf{w}}_{R,k}\right) + \tilde{\mathbf{w}}_{D,k}, \tag{2}$$

where

- $\mathbf{H}_{R,k} \in \mathbb{C}^{N\times N}$ is the MIMO channel matrix between R and D on subcarrier k such that any element of $\mathbf{H}_{R,k}$, e.g., $(n, \bar{n})$th element, $[\mathbf{H}_{R,k}]_{n,\bar{n}}$, represents the sub-channel k between the transmit antenna n of R and the receive antenna $\bar{n}$ of D, i.e. $[\mathbf{H}_{R,k}]_{n,\bar{n}}$, $k = \{1, \ldots, K\}$ is obtained by evaluating the K-point FFT of $\mathbf{g}_R^{n,\bar{n}}$,
- $\tilde{\mathbf{w}}_{D,k} \in \mathbb{C}^N$ is the additive zero-mean Gaussian noise with covariance $\boldsymbol{\mathcal{R}}_D = \sigma_D \mathbf{I}_N$, and σ_D is the noise variance at each receive antenna of D.

[2]FFT operation at the receiver does not change the noise covaraince.

Without loss of generality, the channel matrices $\mathbf{H}_{S,k}$ and $\mathbf{H}_{R,k}$ are assumed nonsingular, which admit the singular value decomposition (SVD)

$$\mathbf{H}_{S,k} = \mathbf{V}_{S,k}\mathbf{\Lambda}_{S,k}\mathbf{U}_{S,k}, \tag{3a}$$
$$\mathbf{H}_{R,k} = \mathbf{U}_{R,k}\mathbf{\Lambda}_{R,k}\mathbf{V}_{R,k}, \tag{3b}$$

where

$$\mathbf{\Lambda}_{S,k} = \text{diag}\{\sqrt{h_{S,k,n}}\}_{n=1}^N, \tag{4a}$$
$$\mathbf{\Lambda}_{R,k} = \text{diag}\{\sqrt{h_{R,k,n}}\}_{n=1}^N, \tag{4b}$$

and

- $\mathbf{V}_{S,k}$, $\mathbf{V}_{R,k}$, $\mathbf{U}_{S,k}$, and $\mathbf{U}_{R,k}$ are unitary matrices of dimension $N \times N$;
- $\{h_{S,k,n}\}_{n=1}^N$ and $\{h_{R,k,n}\}_{n=1}^N$ are the eigenvalues of $\mathbf{H}_{S,k}\mathbf{H}_{S,k}^H$ and $\mathbf{H}_{R,k}^H\mathbf{H}_{R,k}$, respectively. The factors $\sqrt{h_{S,k,n}} \in \mathbb{R}$ and $\sqrt{h_{R,k,n}} \in \mathbb{R}$ can be seen as channel gains from S to R and from R to D over subcarrier k and spatial channel n.

Based on the channel decomposition in (3), the precoding matrix and the relay processing matrix can be set as follows:

$$\mathbf{\Psi}_k = \mathbf{U}_{S,k}^H \mathbf{\Gamma}_{S,k} \tag{5a}$$
$$\mathbf{F}_k = \mathbf{V}_{R,k}^H \mathbf{\Gamma}_{R,k} \mathbf{V}_{S,k}^H, \tag{5b}$$

where

$$\mathbf{\Gamma}_{S,k} \triangleq \text{diag}\{\sqrt{p_{ID,k,n}}\}_{n=1}^N, \tag{6a}$$
$$\mathbf{\Gamma}_{R,k} \triangleq \text{diag}\{\sqrt{\zeta_{k,n}}\sqrt{p_{R,k,n}}\}_{n=1}^N, \tag{6b}$$

and

- $p_{ID,k,n}$ is the power allocated to transmit the source signal $s_{ID,k,n}$ over subcarrier k and spatial channel n, $n \in \{1, \ldots, N\}$;
- $p_{R,k,n}$ is the power allocated to the relay to forward the source signal over subcarrier k and spatial channel n;
- $\zeta_{k,n}$ is the scaling (normalization) factor at R to ensure transmit power of $p_{R,k,n}$ over subcarrier k and spatial channel n.

The list of frequently used symbols with their definition is provided in Table I. Use the matrix decompositions in (3) and (5) to rewrite (1) to

$$\mathbf{y}_{R,k} = \mathbf{\Lambda}_{S,k}\mathbf{\Gamma}_{S,k}\mathbf{s}_{ID,k} + \mathbf{w}_{R,k}, \tag{7}$$

where $\mathbf{y}_{R,k} = \mathbf{V}_{S,k}^H\tilde{\mathbf{y}}_{R,k}$, and $\mathbf{w}_{R,k} = \mathbf{V}_{S,k}^H\tilde{\mathbf{w}}_{R,k}$ is a noise vector with zero mean and covariance $= \mathbf{V}_{S,k}^H\boldsymbol{\mathcal{R}}_R\mathbf{V}_{S,k}$, which is equal to the covariance $\boldsymbol{\mathcal{R}}_R = \sigma_R\mathbf{I}_N$ due to unitary matrix $\mathbf{V}_{S,k}$.

Similarly, (2), can be written to

$$\mathbf{y}_{D,k} = \mathbf{\Lambda}_{R,k}\mathbf{\Gamma}_{R,k}\mathbf{\Lambda}_{S,k}\mathbf{\Gamma}_{S,k}\mathbf{s}_{ID,k} + \mathbf{\Lambda}_{R,k}\mathbf{\Gamma}_{R,k}\mathbf{w}_{R,k} + \mathbf{w}_{D,k} \tag{8}$$

where $\mathbf{y}_{D,k} = \mathbf{U}_{R,k}^H\tilde{\mathbf{y}}_{D,k}$, and $\mathbf{w}_{D,k} = \mathbf{U}_{R,k}^H\tilde{\mathbf{w}}_{D,k}$ is a noise vector with zero mean and covariance $= \mathbf{U}_{R,k}^H\boldsymbol{\mathcal{R}}_D\mathbf{U}_{R,k}$,

TABLE I
LIST OF FREQUENTLY USED SYMBOLS WITH THEIR DEFINITIONS

Symbols	Definition
$h_{S,k,n}$	channel power gain from S to R over subcarrier k and spatial channel n
$h_{R,k,n}$	channel power gain from R to D over subcarrier k and spatial channel n
$h_{E,n}$	channel power gain from E to R over spatial channel n
$p_{R,k,n}$	power allocated to R to forward the source information over subcarrier k and spatial channel n
$p_{ID,k,n}$	power allocated to S to transmit source information data over subcarrier k and spatial channel n
$p_{EH,n}$	power allocated to E to transmit energy signal to R over spatial channel n

which is equal to the covariance $\boldsymbol{\mathcal{R}}_D = \sigma_D \mathbf{I}_N$ due to unitary matrix $\mathbf{U}_{R,k}$.

Using (4) and (6) and the fact that the MIMO channel on the subcarrier k is decomposed to N spatial parallel channels, (7) can be further simplified to

$$y_{R,k,n} = \sqrt{h_{S,k,n}}\sqrt{p_{ID,k,n}} s_{ID,k,n} + \sqrt{\sigma_R} w_{R,k,n}, \quad (9)$$

where $y_{R,k,n}$ is the received signal at R (during the first stage) over subcarrier k and spatial channel n, $s_{ID,k,n}$ is the information data on the subcarrier k and the transmit antenna n such that $\mathbb{E}(|s_{ID,k,n}|^2) = 1$, $w_{R,k,n}$ is the normalized noise such that $\mathbb{E}(|w_{R,k,n}|^2) = 1$, $p_{ID,k,n}$ is defined below (6), and $\sqrt{h_{S,k,n}} \in \mathbb{R}$ is defined from (4).

Similarly, (8) can be further simplified to

$$\begin{aligned} y_{D,k,n} = {} & \sqrt{h_{R,k,n}} \sqrt{\frac{p_{R,k,n}}{h_{S,k,n} p_{ID,k,n} + \sigma_R}} \\ & \times \left(\sqrt{h_{S,k,n} p_{ID,k,n}} s_{ID,k,n} + \sqrt{\sigma_R} w_{R,k,n} \right) \\ & + \sqrt{\sigma_D} w_{D,k,n}, \end{aligned} \quad (10)$$

where $y_{D,k,n}$ is the received signal at D over subcarrier k and spatial channel n, $w_{D,k,n}$ is the normalized noise such that $\mathbb{E}(|w_{D,k,n}|^2) = 1$, $p_{R,k,n}$ is defined from (6), and $\sqrt{h_{R,k,n}} \in \mathbb{R}$ is defined from (4). In (10), $\zeta_{k,n} = \frac{1}{h_{S,k,n} p_{ID,k,n} + \sigma_R}$ is the relay power normalization factor.

Using (10), the signal-to-noise ratio (SNR) at the destination is given by

$$\begin{aligned} \mathrm{SNR}_D &= \frac{h_{R,k,n} p_{R,k,n} h_{S,k,n} p_{ID,k,n}}{(h_{S,k,n} p_{ID,k,n} + \sigma_R)\left(\frac{h_{R,k,n} p_{R,k,n} \sigma_R}{h_{S,k,n} p_{ID,k,n} + \sigma_R} + \sigma_D \right)} \\ &= \frac{h_{R,k,n} p_{R,k,n} h_{S,k,n} p_{ID,k,n}}{h_{R,k,n} p_{R,k,n} \sigma_R + (h_{S,k,n} p_{ID,k,n} + \sigma_R)\sigma_D} \\ &= \frac{(h_{S,k,n}/\sigma_R) p_{ID,k,n} (h_{R,k,n}/\sigma_D) p_{R,k,n}}{1 + (h_{S,k,n}/\sigma_R) p_{ID,k,n} + (h_{R,k,n}/\sigma_D) p_{R,k,n}}. \end{aligned}$$

B. Energy Processing

During the second stage, E transmits a dedicated energy signal to R, while R also receives interference from its own transmission. Let $\mathbf{H}_E \in \mathbb{C}^{N \times N}$ be the time-domain MIMO channel matrix between E and R, i.e., $[\mathbf{H}_E]_{n,\bar{n}} = g_E^{n,\bar{n}}$, and $\mathbf{H}_{LI} \in \mathbb{C}^{N \times N}$ be the time-domain self-loop interference channel matrix at R. The received time-domain signal at R during the second communication phase is given by

$$\tilde{\mathbf{y}}_{EH,i} = \mathbf{H}_E \tilde{\mathbf{s}}_{EH,i} + \mathbf{H}_{LI} \mathbf{x}_{R,i} + \tilde{\mathbf{w}}_{R,i}, \quad (11)$$

where

- $i = \{1, 2, \ldots, K\}$ denotes the time index such that $[\tilde{\mathbf{y}}_{EH,1}, \tilde{\mathbf{y}}_{EH,2}, \ldots, \tilde{\mathbf{y}}_{EH,K}]$ represents the received time-domain signal over one OFDM symbol duration,
- $\tilde{\mathbf{s}}_{EH,i} = \boldsymbol{\Psi}_{EH} \mathbf{s}_{EH,i}$ such that $\boldsymbol{\Psi}_{EH} \in \mathbb{C}^{N \times N}$ is the transmit precoding matrix at the E, $\mathbf{s}_{EH,i} \in \mathbb{C}^N$ is the transmitted energy signal such that $\mathbb{E}(|\mathbf{s}_{EH,i}|^2) = \mathbf{1}^{N \times 1}$
- $\tilde{\mathbf{w}}_{R,i} \in \mathbb{C}^N$ is the additive zero-mean Gaussian noise with covariance $\boldsymbol{\mathcal{R}}_R = \sigma_R \mathbf{I}_N$, σ_R is the noise variance at each receive antenna at R, and
- $\mathbf{x}_{R,i} \in \mathbb{C}^N$ is the transmitted signal by the R during second communication phase, which is given by the K-point IFFT of the signal $\mathbf{F}_k \left(\mathbf{H}_{S,k} \tilde{\mathbf{s}}_{ID,k} + \tilde{\mathbf{w}}_{R,k} \right)$ (see eq. (2)), i.e.,

$$\mathbf{x}_{R,i} = \frac{1}{\sqrt{K}} \sum_{k=1}^{K} \mathbf{F}_k \left(\mathbf{H}_{S,k} \tilde{\mathbf{s}}_{ID,k} + \tilde{\mathbf{w}}_{R,k} \right) e^{j \frac{2\pi}{K}(k-1)(i-1)} \quad (12)$$

Let the SVD of the channel matrix $\mathbf{H}_E$ be given by

$$\mathbf{H}_E = \mathbf{V}_E \boldsymbol{\Lambda}_E \mathbf{U}_E$$

where $\boldsymbol{\Lambda}_E \triangleq \mathrm{diag}\{\sqrt{h_{E,n}}\}_{n=1}^N$, $\mathbf{V}_E$ and $\mathbf{U}_E$ are unitary matrices of dimensions and $N \times N$, and $\{h_{E,n}\}_{n=1}^N$ are the eigenvalues of $\mathbf{H}_E \mathbf{H}_E^H$. The transmit precoding matrix at E is given by

$$\boldsymbol{\Psi}_{EH} = \mathbf{U}_E^H \boldsymbol{\Gamma}_E$$

where $\boldsymbol{\Gamma}_E = \mathrm{diag}\{\sqrt{p_{EH,n}}\}_{n=1}^N$ and $p_{EH,n}$ is the power allocated to transmit the energy signal over spatial channel n. Thus, the (11) of the received signal at R during second communication phase can be written as

$$\mathbf{y}_{EH,i} = \underbrace{\boldsymbol{\Lambda}_E \boldsymbol{\Gamma}_E \mathbf{s}_{EH,i}}_{\text{from energy source}} + \underbrace{\mathbf{V}_E^H \mathbf{H}_{LI} \mathbf{x}_{R,i}}_{\text{SI from relay}} + \underbrace{\mathbf{V}_E^H \tilde{\mathbf{w}}_{R,i}}_{\text{noise}}, \quad (13)$$

for $\mathbf{y}_{EH,i} = \mathbf{V}_E^H \tilde{\mathbf{y}}_{EH,i}$. Given that the transmit power at R over subcarrier k and spatial channel n is $p_{R,k,n}$, the power of the transmitted signal at the relay $\mathbf{x}_{R,i}$ is given by $\sum_{k=1}^K \sum_{n=1}^N p_{R,k,n}$. Thus, the power harvested at the R due to the self-loop interference from its own transmission (second factor in (13) can be expressed as

$$\eta \gamma_{LI} \sum_{k=1}^{K} \sum_{n=1}^{N} p_{R,k,n},$$

where γ_{LI} is the self-loop path gain or in other words, it is the inverse of the path loss of the self-loop channel [19] and η is the energy harvesting efficiency. Thus, the recycled energy due to self-loop interference depends on γ_{LI} and η.

Using (13), the power harvested by the relay (combined from all the receive antennas) during the second communication phase is given by

$$e = \eta \sum_{n=1}^{N} \left(h_{E,n} p_{EH,n} + \gamma_{LI} \sum_{k=1}^{K} p_{R,k,n} \right). \tag{14}$$

Note that in (14), the noise factor (third factor in (13) has been ignored as it results in negligible harvested energy. In order to ensure that the total transmitted power by the relay does not exceed the total harvested power, the following constraint is imposed:

$$\sum_{k=1}^{K} \sum_{n=1}^{N} p_{R,k,n} \leq e. \tag{15}$$

C. Problem Formulation

By setting

$$a_{k,n} = \frac{h_{S,k,n}}{\sigma_R}, \quad b_{k,n} = \frac{h_{R,k,n}}{\sigma_D}, \; c_n = \frac{h_{E,n}}{\sigma_R}, \tag{16}$$

the sum-rate maximization problem at the destination can be formulated as

$$\max_{(\mathbf{p}_{ID}, \mathbf{p}_{EH}, \mathbf{p}_R)} \; f(\mathbf{p}_{ID}, \mathbf{p}_R)$$

$$\triangleq \sum_{k=1}^{K} \sum_{n=1}^{N} \ln\left(1 + \frac{a_{k,n} p_{ID,k,n} b_{k,n} p_{R,k,n}}{1 + a_{k,n} p_{ID,k,n} + b_{k,n} p_{R,k,n}}\right) \tag{17a}$$

$$\text{s.t.} \sum_{k=1}^{K} \sum_{n=1}^{N} p_{ID,k,n} + \sum_{n=1}^{N} p_{EH,n} \leq P,$$

$$p_{ID,k,n} \geq 0, \quad p_{EH,n} \geq 0, \; p_{R,k,n} \geq 0, \tag{17b}$$

$$\sum_{k=1}^{K} \sum_{n=1}^{N} p_{R,k,n} \leq \eta \sum_{n=1}^{N} \left(\sigma_R c_n p_{EH,n} + \gamma_{LI} \sum_{k=1}^{K} p_{R,k,n} \right), \tag{17c}$$

where P is the total transmit power budget, $\mathbf{p}_{ID} \triangleq \{p_{ID,k,n} : k = 1, \ldots, K; n = 1, \ldots, N\}$, and similarly, $\mathbf{p}_{EH} \triangleq \{p_{EH,n} : n = 1, \ldots, N\}$ and $\mathbf{p}_R \triangleq \{p_{R,k,n} : k = 1, \ldots, K; n = 1, \ldots, N\}$. Note that it is due to the use of OFDM and MIMO channel decomposition that the design of precoding and relaying matrices in a MIMO communication setup is simplified to that of scalar power allocation problem over multiple subcarriers and spatial channels.

Apart from the non-concave objective function (17a), the main issue is the high dimension of (17). Since the number K of subcarriers is up to 4096, the number of optimization variables in (17) can easily exceed ten thousands, making (17) large-scale nonconvex optimization problem. *Our main goal to develop a method that admits a closed-form solution* at each iteration.

III. Proposed Solution

In this section, we propose a solution to solve the non-convex optimization problem (17). In what follows, define

$$f_{k,n}\left(p_{ID,k,n}, p_{R,k,n}\right) \triangleq \ln\left(1 + \frac{a_{k,n} p_{ID,k,n} b_{k,n} p_{R,k,n}}{1 + a_{k,n} p_{ID,k,n} + b_{k,n} p_{R,k,n}}\right) \tag{18}$$

and decompose it as

$$f_{k,n}\left(p_{ID,k,n}, p_{R,k,n}\right) = \ln(1 + a_{k,n} p_{ID,k,n}) + \ln(1 + b_{k,n} p_{R,k,n}) - \ln(1 + a_{k,n} p_{ID,k,n} + b_{k,n} p_{R,k,n}). \tag{19}$$

The first two terms in (19) are concave while the last term is convex, so the objective function (17a) is a d.c. (difference of two convex) function [44]. As such in principle (17) can be addressed by d.c. iterations (DCI) [45] as follows. Let $(\mathbf{p}_{ID}^{(\kappa)}, \mathbf{p}_{EH}^{(\kappa)}, \mathbf{p}_R^{(\kappa)})$ be a feasible point for (17) that is found from the $(\kappa-1)$th iteration. By linearizing the last term in (19) around $\left(\mathbf{p}_{ID}^{(\kappa)}, \mathbf{p}_R^{(\kappa)}\right)$ while keeping the first two terms (19) one can easily obtain a lower bounding concave approximation of the objective function (17a) as

$$f_{DC}^{(\kappa)}(\mathbf{p}_{ID}, \mathbf{p}_R) \triangleq \sum_{k=1}^{K} \sum_{n=1}^{N} \Big[\ln(1 + a_{k,n} p_{ID,k,n}) + \ln(1 + b_{k,n} p_{R,k,n}) - \ln(1 + a_{k,n} p_{ID,k,n}^{(\kappa)} + b_{k,n} p_{R,k,n}^{(\kappa)}) - \frac{a_{k,n}(p_{ID,k,n} - p_{ID,k,n}^{(\kappa)}) + b_{k,n}(p_{R,k,n} - p_{R,k,n}^{(\kappa)})}{1 + a_{k,n} p_{ID,k,n}^{(\kappa)} + b_{k,n} p_{R,k,n}^{(\kappa)}} \Big]. \tag{20}$$

DCI [45] solves the following problem of a logarithmic function optimization under convex constraints at the κth iteration to generate the next feasible point $(\mathbf{p}_{ID}^{(\kappa+1)}, \mathbf{p}_{EH}^{(\kappa+1)}, \mathbf{p}_R^{(\kappa+1)})$ for (17):

$$\max_{(\mathbf{p}_{ID}, \mathbf{p}_{EH}, \mathbf{p}_R)} f_{DC}^{(\kappa)}(\mathbf{p}_{ID}, \mathbf{p}_R) \;\; \text{s.t. (17b), (17b), (17c).} \tag{21}$$

However, there is no solver of polynomial complexity for (21). Furthermore, using the following lower bounding concave approximation of the objective function (17a) [46]:

$$f_{QD}^{(\kappa)}(\mathbf{p}_{ID}, \mathbf{p}_R) \triangleq \sum_{k=1}^{K} \sum_{n=1}^{N} \Bigg[\frac{a_{k,n}}{1 + a_{k,n} p_{ID,k,n}^{(\kappa)}} \left(p_{ID,k,n}^{(\kappa)} - \frac{(p_{ID,k,n}^{(\kappa)})^2}{p_{ID,k,n}} \right) + \frac{b_{k,n}}{1 + b_{k,n} p_{R,k,n}^{(\kappa)}} \left(p_{R,k,n}^{(\kappa)} - \frac{(p_{R,k,n}^{(\kappa)})^2}{p_{R,k,n}} \right) + f_{k,n}(p_{ID,k,n}^{(\kappa)} p_{R,k,n}^{(\kappa)}) - \frac{a_{k,n}(p_{ID,k,n} - p_{ID,k,n}^{(\kappa)}) + b_{k,n}(p_{R,k,n} - p_{R,k,n}^{(\kappa)})}{1 + a_{k,n} p_{ID,k,n}^{(\kappa)} + b_{k,n} p_{R,k,n}^{(\kappa)}} \Bigg] \tag{22}$$

leads to solving the following convex quadratic optimization at the κth iteration instead of (21) to generate the next feasible $(\mathbf{p}_{ID}^{(\kappa+1)}, \mathbf{p}_{EH}^{(\kappa+1)}, \mathbf{p}_R^{(\kappa+1)})$ for (17):

$$\max_{(\mathbf{p}_{ID}, \mathbf{p}_{EH}, \mathbf{p}_R)} f_{QD}^{(\kappa)}(\mathbf{p}_{ID}, \mathbf{p}_R) \;\; \text{s.t. (17b), (17b), (17c).} \tag{23}$$

Both (21) and (23) are convex but very large scale problems. The computational complexity of (23) is [47]:

$$\mathcal{O}\left(((2KN + N)^3 (2KN + N + 2))\right), \tag{24}$$

i.e. it is more computationally tractable than (21). However, this computational complexity is still too high for practical application. Even with only $K = 64$ subcarriers and $N = 4$ antennas, it takes more than half an hour for (21)-based iterations and around 3 minutes for (23)-based iterations on a core-i5 machine (8 GB RAM) using MATLAB and CVX solver to find the optimal solution.

Leaving aside its practical issue as mentioned in the Introduction, the work [20] considered the design of robust non-linear transceivers (source precoding, MIMO relaying, and receiver matrices) to minimize the mean-squared error at the destination end in the presence of channel uncertainty. Alternating optimization, which optimizes one of these three matrices with other two held fixed, is used to address the posed optimization problem. The alternating optimization in the source precoding matrix is still nonconvex, for which the DCI [45] is also revoked. It should be noted that the solution founded by alternating optimization approach does not necessarily satisfy a necessary optimality condition. Such an optimization problem as posed in [20] should be much more efficiently addressed by the matrix optimization techniques in [48], [49], which simultaneously optimize all the matrix variables in each iteration, avoiding alternating optimization.

We now develop a new lower bounding concave approximation for the objective function (17a) as well as a new inner convex approximation for the polytopic constraints (17b)-(17c), which lead to a closed-form of the optimal solution at each iteration.

As before, let $(\mathbf{p}_{ID}^{(\kappa)}, \mathbf{p}_{EH}^{(\kappa)}, \mathbf{p}_{R}^{(\kappa)})$ be a feasible point for (17) that is found from the $(\kappa-1)$th iteration.

A. Lower Bounding Concave Approximation for the Objective Function (17a) *at the κth Iteration*

By using the inequality (45) in the appendix:

$$\begin{aligned}&\ln(1+a_{k,n}p_{ID,k,n})\\&\quad\geq \ln(1+a_{k,n}p_{ID,k,n}^{(\kappa)})\\&\qquad+\frac{a_{k,n}p_{ID,k,n}^{(\kappa)}}{1+a_{k,n}p_{ID,k,n}^{(\kappa)}}\left(\ln p_{ID,k,n}-\ln p_{ID,k,n}^{(\kappa)}\right)\end{aligned}\tag{25}$$

and

$$\begin{aligned}&\ln(1+b_{k,n}p_{R,k,n})\\&\quad\geq \ln(1+b_{k,n}p_{R,k,n}^{(\kappa)})\\&\qquad+\frac{b_{k,n}p_{R,k,n}^{(\kappa)}}{1+b_{k,n}p_{R,k,n}^{(\kappa)}}\left(\ln p_{R,k,n}-\ln p_{R,k,n}^{(\kappa)}\right),\end{aligned}\tag{26}$$

while by using the inequality (43) in the appendix

$$\begin{aligned}&\ln(1+a_{k,n}p_{ID,k,n}+b_{k,n}p_{R,k,n})\\&\quad\leq \ln(1+a_{k,n}p_{ID,k,n}^{(\kappa)}+b_{k,n}p_{R,k,n}^{(\kappa)})\\&\qquad+\frac{a_{k,n}(p_{ID,k,n}-p_{ID,k,n}^{(\kappa)})+b_{k,n}(p_{R,k,n}-p_{R,k,n}^{(\kappa)})}{1+a_{k,n}p_{ID,k,n}^{(\kappa)}+b_{k,n}p_{R,k,n}^{(\kappa)}}.\end{aligned}\tag{27}$$

Therefore,

$$\begin{aligned}&f_{k,n}(p_{ID,k,n},p_{R,k,n})\\&\quad\geq f_{k,n}^{(\kappa)}(p_{ID,k,n},p_{R,k,n})\\&\quad\triangleq \alpha_{k,n}^{(\kappa)}+\beta_{k,n}^{(\kappa)}\ln p_{ID,k,n}-\chi_{k,n}^{(\kappa)}p_{ID,k,n}\\&\qquad+\delta_{k,n}^{(\kappa)}\ln p_{R,k,n}-\gamma_{k,n}^{(\kappa)}p_{R,k,n},\end{aligned}\tag{28}$$

where

$$\begin{aligned}\alpha_{k,n}^{(\kappa)}&=\ln\left(1+\frac{a_{k,n}p_{ID,k,n}^{(\kappa)}b_{k,n}p_{R,k,n}^{(\kappa)}}{1+a_{k,n}p_{ID,k,n}^{(\kappa)}+b_{k,n}p_{R,k,n}^{(\kappa)}}\right)\\&\quad-\frac{a_{k,n}p_{ID,k,n}^{(\kappa)}}{1+a_{k,n}p_{ID,k,n}^{(\kappa)}}\ln p_{ID,k,n}^{(\kappa)}-\frac{b_{k,n}p_{R,k,n}^{(\kappa)}}{1+b_{k,n}p_{R,k,n}^{(\kappa)}}\ln p_{R,k,n}^{(\kappa)}\\&\quad+\frac{1}{1+a_{k,n}p_{ID,k,n}^{(\kappa)}+b_{k,n}p_{R,k,n}^{(\kappa)}}\\&\quad\times\left(a_{k,n}p_{ID,k,n}^{(\kappa)}+b_{k,n}p_{R,k,n}^{(\kappa)})\right),\end{aligned}\tag{29a}$$

$$\beta_{k,n}^{(\kappa)}=\frac{a_{k,n}p_{ID,k,n}^{(\kappa)}}{1+a_{k,n}p_{ID,k,n}^{(\kappa)}}>0,\tag{29b}$$

$$\chi_{k,n}^{(\kappa)}=\frac{1}{1+a_{k,n}p_{ID,k,n}^{(\kappa)}+b_{k,n}p_{R,k,n}^{(\kappa)}}a_{k,n}>0,\tag{29c}$$

$$\delta_{k,n}^{(\kappa)}=\frac{b_{k,n}p_{R,k,n}^{(\kappa)}}{1+b_{k,n}p_{R,k,n}^{(\kappa)}}>0,\tag{29d}$$

$$\gamma_{k,n}^{(\kappa)}=\frac{1}{1+a_{k,n}p_{ID,k,n}^{(\kappa)}+b_{k,n}p_{R,k,n}^{(\kappa)}}b_{k,n}>0.\tag{29e}$$

Note that $f_{k,n}^{(\kappa)}(p_{ID,k,n},p_{R,k,n})$ is a concave function, which matches with $f_{k,n}(p_{ID,k,n},p_{R,k,n})$ at $(p_{ID,k,n}^{(\kappa)},p_{R,k,n}^{(\kappa)})$, i.e. $f_{k,n}(p_{ID,k,n}^{(\kappa)},p_{R,k,n}^{(\kappa)})=f_{k,n}^{(\kappa)}(p_{ID,k,n}^{(\kappa)},p_{R,k,n}^{(\kappa)})$. Consequently, the function

$$f^{(\kappa)}(\mathbf{p}_{ID},\mathbf{p}_R)\triangleq\sum_{k=1}^{K}\sum_{n=1}^{N}f_{k,n}^{(\kappa)}(p_{ID,k,n},p_{R,k,n})$$

is a lower bounding concave approximation of $f(\mathbf{p}_{ID},\mathbf{p}_R)$:

$$f(\mathbf{p}_{ID},\mathbf{p}_R)\geq f^{(\kappa)}(\mathbf{p}_{ID},\mathbf{p}_R)\quad\forall\,(\mathbf{p}_{ID},\mathbf{p}_R),\tag{30}$$

and matches with $f(\mathbf{p}_{ID},\mathbf{p}_R)$ at $(\mathbf{p}_{ID}^{(\kappa)},\mathbf{p}_R^{(\kappa)})$:

$$f(\mathbf{p}_{ID}^{(\kappa)},\mathbf{p}_R^{(\kappa)})=f^{(\kappa)}(\mathbf{p}_{ID}^{(\kappa)},\mathbf{p}_R^{(\kappa)}).\tag{31}$$

B. Inner Approximation of Polytopic Constraints at the κth Iteration

Observe that $p_{EH,n}$ appears only in the polytopic constraints (17b) and (17c). Now, note that

$$\begin{aligned}p_{EH,n}^2+(p_{EH,n}^{(\kappa)})^2-2p_{EH,n}p_{EH,n}^{(\kappa)}&=(p_{EH,n}-p_{EH,n}^{(\kappa)})^2\\&\geq 0\end{aligned}$$

leading to

$$p_{EH,n}\leq 0.5\left(p_{EH,n}^2/p_{EH,n}^{(\kappa)}+p_{EH,n}^{(\kappa)}\right),$$

we innerly approximate the polytopic constraint (17b) by the convex quadratic constraint

$$\sum_{k=1}^{K}\sum_{n=1}^{N} p_{ID,k,n} + 0.5\sum_{n=1}^{N}\left(\frac{p_{EH,n}^2}{p_{EH,n}^{(\kappa)}} + p_{EH,n}^{(\kappa)}\right) \le P. \quad (32)$$

Indeed, it is obvious that any feasible point for (32) is also feasible for (17b).

C. Closed-Form Solution at the κth Iteration

At the κth iteration, we solve the following convex optimization problem to generate the next iterative feasible point $(\mathbf{p}_{ID}^{(\kappa+1)}, \mathbf{p}_{EH}^{(\kappa+1)}, \mathbf{p}_{R}^{(\kappa+1)})$ for (17):

$$\max_{(\mathbf{p}_{ID},\mathbf{p}_{EH},\mathbf{p}_R)} \; f^{(\kappa)}(\mathbf{p}_{ID}, \mathbf{p}_R) \;\; \text{s.t. (17c), (17b), (32).} \quad (33)$$

The difference between the convex problem (33) and the DCI (21) is that the concave functions $\ln(1 + a_{k,n}p_{ID,k,n})$ and $\ln(1 + b_{k,n}p_{R,k,n})$ in the objective function of the former are further approximated by other concave functions, and the polytopic constraint (17b) is innerly approximated by the convex constraint (32). These approximations help to ease the process of finding a closed form solution of (33).

The Lagrangian of problem (33) is given by

$$\begin{aligned}
&\mathcal{L}(\mathbf{p}_{ID}, \mathbf{p}_{EH}, \mathbf{p}_R, \lambda_1, \lambda_2)\\
&= \sum_{k=1}^{K}\sum_{n=1}^{N} f_{k,n}^{(\kappa)}(p_{ID,k,n}, p_{R,k,n})\\
&\quad - \lambda_1\left(\sum_{k=1}^{K}\sum_{n=1}^{N} p_{ID,k,n} + \frac{1}{2}\sum_{n=1}^{N}\left(\frac{p_{EH,n}^2}{p_{EH,n}^{(\kappa)}} + p_{EH,n}^{(\kappa)}\right) - P\right)\\
&\quad - \lambda_2\left((1-\eta\gamma_{LI})\sum_{k=1}^{K}\sum_{n=1}^{N} p_{R,k,n} - \eta\sum_{n=1}^{N}\sigma_R c_n p_{EH,n}\right)\\
&\quad + \nu_{k,n}p_{ID,k,n} + \bar{\nu}_{k,n}p_{R,k,n} + \hat{\nu}_n p_{EH,n},
\end{aligned}$$

where $\lambda_1 \ge 0$ and $\lambda_2 \ge 0$ are the Lagrange multipliers corresponding to the constraints (32) and (17c), respectively, while $\nu_{k,n} \ge 0$, $\bar{\nu}_{k,n} \ge 0$, and $\hat{\nu}_n \ge 0$ are the Lagrange multipliers corresponding to the power constraints $p_{ID,k,n} \ge 0$, $p_{R,k,n} \ge 0$, and $p_{EH,n} \ge 0$, respectively, in (17b). We set the Lagrange multipliers $\nu_{k,n} = 0$, $\bar{\nu}_{k,n} = 0$, and $\hat{\nu}_n = 0$ to satisfy the complementary slackness, $\nu_{k,n}p_{ID,k,n} = 0$, $\bar{\nu}_{k,n}p_{R,k,n} = 0$, and $\hat{\nu}_n p_{EH,n} = 0$, for all $k = 1, \ldots, K$, $n = 1, \ldots, N$, in Karush-Kuhn-Tucker (KKT) conditions.

The optimal solution of (33) thus satisfies

$$\begin{aligned}
&\frac{\partial\mathcal{L}(\mathbf{p}_{ID}, \mathbf{p}_{EH}, \mathbf{p}_R, \lambda_1, \lambda_2)}{\partial p_{EH,n}} = 0\\
&\Leftrightarrow -\frac{\lambda_1 p_{EH,n}}{p_{EH,n}^{(\kappa)}} + \lambda_2\eta\sigma_R c_n = 0 \quad (34)\\
&\Leftrightarrow p_{EH,n} = \lambda_2\eta\sigma_R c_n p_{EH,n}^{(\kappa)}/\lambda_1, \quad (35)
\end{aligned}$$

and

$$\begin{aligned}
&\frac{\partial\mathcal{L}(\mathbf{p}_{ID}, \mathbf{p}_{EH}, \mathbf{p}_R, \lambda_1, \lambda_2)}{\partial p_{ID,k,n}} = 0\\
&\Leftrightarrow \frac{\beta_{k,n}^{(\kappa)}}{p_{ID,k,n}} - \chi_{k,n}^{(\kappa)} - \lambda_1 = 0\\
&\Leftrightarrow p_{ID,k,n} = \frac{\beta_{k,n}^{(\kappa)}}{\chi_{k,n}^{(\kappa)} + \lambda_1}, \quad (36)
\end{aligned}$$

and

$$\begin{aligned}
&\frac{\partial\mathcal{L}(\mathbf{p}_{ID}, \mathbf{p}_{EH}, \mathbf{p}_R, \lambda_1, \lambda_2)}{\partial p_{R,k,n}} = 0\\
&\Leftrightarrow \frac{\delta_{k,n}^{(\kappa)}}{p_{R,k,n}} - \gamma_{k,n}^{(\kappa)} - \lambda_2(1-\eta\gamma_{LI}) = 0\\
&\Leftrightarrow p_{R,k,n} = \frac{\delta_{k,n}^{(\kappa)}}{\gamma_{k,n}^{(\kappa)} + \lambda_2(1-\eta\gamma_{LI})}, \quad (37)
\end{aligned}$$

where (35) shows that λ_1 should be strictly positive. To satisfy the complementary slackness under KKT conditions for the constraints (32) and (17c), $\lambda_1 > 0$ and $\lambda_2 > 0$ are chosen such that the constraints (32) and (17c) are met with equality. Thus,

$$\begin{aligned}
&\sum_{k=1}^{K}\sum_{n=1}^{N} p_{ID,k,n} + 0.5\sum_{n=1}^{N}\left(\frac{p_{EH,n}^2}{p_{EH,n}^{(\kappa)}} + p_{EH,n}^{(\kappa)}\right) \le P\\
&\Leftrightarrow \sum_{k=1}^{K}\sum_{n=1}^{N}\frac{\beta_{k,n}^{(\kappa)}}{\chi_{k,n}^{(\kappa)} + \lambda_1} + 0.5\sum_{n=1}^{N} p_{EH,n}^{(\kappa)}\left(\frac{\lambda_2^2\eta^2\sigma_R^2 c_n^2}{\lambda_1^2} + 1\right) = P, \quad (38)
\end{aligned}$$

and

$$\begin{aligned}
&(1-\eta\gamma_{LI})\sum_{k=1}^{K}\sum_{n=1}^{N} p_{R,k,n} = \eta\sum_{n=1}^{N}\sigma_R c_n p_{EH,n}\\
&\Leftrightarrow (1-\eta\gamma_{LI})\sum_{k=1}^{K}\sum_{n=1}^{N}\frac{\delta_{k,n}^{(\kappa)}}{\gamma_{k,n}^{(\kappa)} + \lambda_2(1-\eta\gamma_{LI})}\\
&\quad = \eta\sum_{n=1}^{N}\frac{\lambda_2\sigma_R c_n\eta\sigma_R c_n p_{EH,n}^{(\kappa)}}{\lambda_1}. \quad (39)
\end{aligned}$$

Simultaneously solving (38) and (39) will yield the optimal values of λ_2 and λ_1. From (39), we can get λ_1 expressed as a function of λ_2:

$$\lambda_1 = \frac{\eta\lambda_2}{1-\eta\gamma_{LI}}\frac{\sum_{n=1}^{N}\eta\sigma_R^2 c_n^2 p_{EH,n}^{(\kappa)}}{\sum_{k=1}^{K}\sum_{n=1}^{N}\left(\frac{\delta_{k,n}^{(\kappa)}}{\gamma_{k,n}^{(\kappa)} + \lambda_2(1-\eta\gamma_{LI})}\right)}. \quad (40)$$

Substituting this value of λ_1 into (38), we can solve for λ_2 by using bisection search and finally get λ_1 from (40).

Remark 1: In (25) and (26), we approximate concave functions by other concave functions, which lead to the simple closed forms (36) and (37) and consequently, the analytical formula (40) for determining the Lagrange multiplier λ_1.

Remark 2: It can be easily seen that using the polytopic constraint (17b) cannot reveal a closed-form of $p_{EH,n}$ because the derivative of the corresponding Lagrangian with respect to $p_{EH,n}$ as in (34) is independent of $p_{EH,n}$. That is why we need the inner approximation (32) for (17b) that leads to the closed-form (35) for $p_{EH,n}$.

Algorithm 1 Resource Allocation Algorithm for Rate Maximization Problem (17)

Initialization: Set $\kappa := 0$. Take the initial feasible point $(\mathbf{p}_{EH}^{(0)}, \mathbf{p}_{ID}^{(0)}, \mathbf{p}_{R}^{(0)})$ by using (41).

1: **repeat**
2: Solve for λ_1 and λ_2 using (38) and (40) (the details are given below (39)).
3: Update $\left(\mathbf{p}_{EH}^{(\kappa+1)}, \mathbf{p}_{ID}^{(\kappa+1)}, \mathbf{p}_{R}^{(\kappa+1)}\right)$ using the closed-forms (35), (36), and (37).
4: Set $\kappa := \kappa + 1$.
5: **until** Convergence

D. Algorithm and Convergence

The following feasible point $(\mathbf{p}_{EH}^{(0)}, \mathbf{p}_{ID}^{(0)}, \mathbf{p}_{R}^{(0)})$ is taken as the initial point:

$$p_{EH,n}^{(0)} = \frac{0.5P}{N} \tag{41a}$$

$$p_{ID,k,n}^{(0)} = \frac{0.5P}{KN} \tag{41b}$$

$$p_{R,k,n}^{(0)} = \frac{\eta h_{E,n} p_{EH,n}^{(0)}}{K(1-\eta\gamma_{LI})}. \tag{41c}$$

It can be easily seen that all the constraints (17b), (17b), and (17c) are met. Algorithm 1 outlines the steps to solve the rate maximization problem (17). The computational complexity of Algorithm 1 is

$$\mathcal{O}(KN), \tag{42}$$

as it just involves $5N$, $2KN$, and $5KN$ addition or multiplication operations to update $\left(\mathbf{p}_{EH}^{(\kappa+1)}, \mathbf{p}_{ID}^{(\kappa+1)}, \mathbf{p}_{R}^{(\kappa+1)}\right)$ using (35), (36), and (37), respectively, over the κth iteration, while the algorithm converges within few iteration (around $15-20$) and we are dealing with $K = 1024$ subcarriers.

In the following, we show that Algorithm 1 generates a sequence $\{\mathbf{p}_{EH}^{(\kappa)}, \mathbf{p}_{ID}^{(\kappa)}, \mathbf{p}_{R}^{(\kappa)}\}$ of improved feasible points for (17). It is clear from (31) that

$$f(\mathbf{p}_{ID}^{(\kappa)}, \mathbf{p}_{R}^{(\kappa)}) = f^{(\kappa)}(\mathbf{p}_{ID}^{(\kappa)}, \mathbf{p}_{R}^{(\kappa)}).$$

Furthermore,

$$f^{(\kappa)}(\mathbf{p}_{ID}^{(\kappa+1)}, \mathbf{p}_{R}^{(\kappa+1)}) > f^{(\kappa)}(\mathbf{p}_{ID}^{(\kappa)}, \mathbf{p}_{R}^{(\kappa)})$$

as far as $\left(\mathbf{p}_{EH}^{(\kappa+1)}, \mathbf{p}_{ID}^{(\kappa+1)}, \mathbf{p}_{R}^{(\kappa+1)}\right) \neq \left(\mathbf{p}_{EH}^{(\kappa)}, \mathbf{p}_{ID}^{(\kappa)}, \mathbf{p}_{R}^{(\kappa)}\right)$, because $(\mathbf{p}_{EH}^{(\kappa+1)}, \mathbf{p}_{ID}^{(\kappa+1)}, \mathbf{p}_{R}^{(\kappa+1)})$ is the optimal solution of (33) while $(\mathbf{p}_{EH}^{(\kappa)}, \mathbf{p}_{ID}^{(\kappa)}, \mathbf{p}_{R}^{(\kappa)})$ is a feasible point for (33). Therefore, by (30),

$$\begin{aligned} f(\mathbf{p}_{ID}^{(\kappa+1)}, \mathbf{p}_{R}^{(\kappa+1)}) &\geq f^{(\kappa)}(\mathbf{p}_{ID}^{(\kappa+1)}, \mathbf{p}_{R}^{(\kappa+1)}) \\ &> f^{(\kappa)}(\mathbf{p}_{ID}^{(\kappa)}, \mathbf{p}_{R}^{(\kappa)}) \\ &= f(\mathbf{p}_{ID}^{(\kappa)}, \mathbf{p}_{R}^{(\kappa)}), \end{aligned}$$

i.e. $(\mathbf{p}_{EH}^{(\kappa+1)}, \mathbf{p}_{ID}^{(\kappa+1)}, \mathbf{p}_{R}^{(\kappa+1)})$ is a better feasible point $(\mathbf{p}_{EH}^{(\kappa)}, \mathbf{p}_{ID}^{(\kappa)}, \mathbf{p}_{R}^{(\kappa)})$ for the original nonconvex optimization problem (17). As such, Algorithm 1 converges at least to a locally optimal solution of (17) [13].

IV. Numerical Results

This section evaluates the performance of the proposed Alg. 1 and also analyses its computational efficiency.

A. The Simulation Setup

We assume $N = 4$ antennas at each node. To model large scale fading, each spatial $L = 16$-tap source-to-relay channel, $\mathbf{g}_S^{n,\bar{n}}$, between any transmit antenna n and receive antenna $\bar{n}$, follows the path loss model $30 + 10\beta\log_{10}(d_{SR})$ and each spatial $L = 16$-tap R-to-S channel, $\mathbf{g}_R^{n,\bar{n}}$, between any transmit antenna n and receive antenna $\bar{n}$, follows the path loss model $30 + 10\beta\log_{10}(d_{RD})$, where the path loss exponent $\beta = 3$, the distance from S-to-R, d_{SR}, is set to 100 meters and unless specified otherwise, the distance from R-to-D, d_{RD}, is also set to 100 meters. On the other hand, the channel between E and R, $g_E^{n,\bar{n}}$ follows the path loss model $30 + 10\beta_E\log_{10}(d_{ER})$, where path loss exponent $\beta_E = 2$, and the distance between E and R, d_{ER} is set to 10 meters. Note that different values for path-loss exponents have been proposed for different type of channel conditions in the literature too [50], [51]. To ensure meaningful wireless power transfer to energy harvesting node, smaller distance with line-of-sight component and hence, smaller value of path-loss exponent are adopted in the literature [51].

To model small scale fading, $\mathbf{g}_S^{n,\bar{n}}$ and $\mathbf{g}_R^{n,\bar{n}}$ follow Rayleigh fading, while $g_E^{n,\bar{n}}$ is assumed to be Rician distributed with Rician factor $\mathcal{K} = 6$ dB. To simulate the effect of frequency selectivity in each spatial multipath channel $\mathbf{g}_S^{n,\bar{n}}$ and $\mathbf{g}_R^{n,\bar{n}}$, we assume an exponential power delay profile with root-mean-square delay spread of $\sigma_{\text{RMS}} = 3\ T_s$, for the symbol time $T_s = 1/B$. In addition, the spatial correlation among the MIMO channels are modeled according to Case B of the 3 GPP I-METRA MIMO channel model [35].

The time-domain multipath channels $\mathbf{g}_S^{n,\bar{n}}$ and $\mathbf{g}_R^{n,\bar{n}}$ are converted to frequency domain via a K-point FFT. Unless specified otherwise, the number of OFDM subcarriers is considered to be $K = 1024$ and the total transmit power budget P is set to 26 dBm. The system bandwidth is set to $B = 1$-MHz and the subcarrier bandwidth is B/K. This subcarrier bandwidth is quite smaller than the coherence bandwidth of $0.02/\sigma_{RMS}$ to ensure flat fading over each subcarrier. In each sub-channel, the power spectral density (noise per unit BW) of additive white Gaussian noise, $\frac{\sigma_R}{B/K}$ and $\frac{\sigma_D}{B/K}$ at each antenna is set to -174 dBm/Hz. Therefore, the total noise power over each subcarrier, e.g., at the relay-receiver, can be found as $\sigma_R = 10^{(-174+30)/10} \times (B/K)$. The correlation between noise samples from different antennas is set to 0.2. The carrier frequency is assumed to be 1 GHz. Unless specified otherwise, the self-loop path gain or SI is set to $\gamma_{LI} = -10$ dB [20], [28], which is justified since there is no need of self-interference attenuation at R for energy recycle at R. The energy harvesting efficiency η is set to 0.5 [17, Table III]. Note that using the aforementioned path loss model and practical simulation setup, the power of the received signal at the relay during second communication phase passes the threshold minimum power requirement (-21 dBm with 13 nm CMOS technology [17]) to carry out EH at the relay.

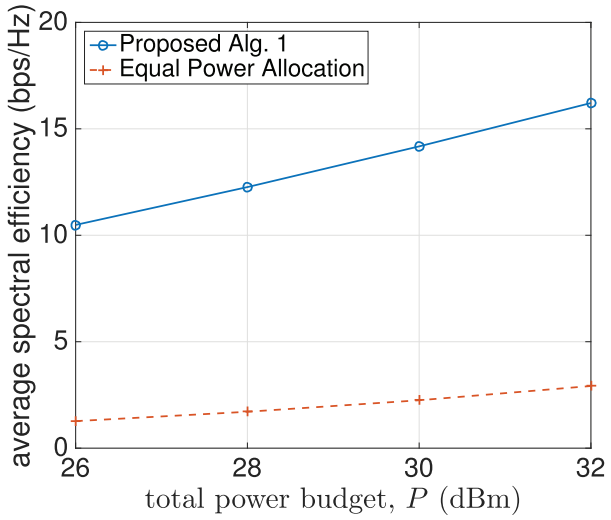

Fig. 3. Average spectral efficiency versus the total power budget P.

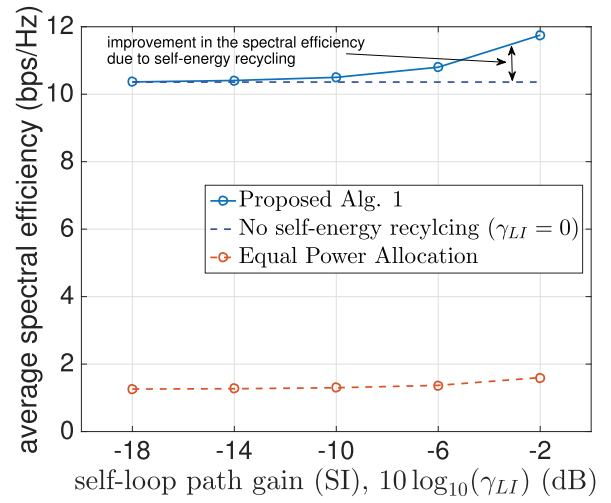

Fig. 4. Average spectral efficiency versus the self-loop path gain (SI) γ_{LI} (evaluated in dB).

The tolerance level for the convergence of Alg. 1 is set to 0.001 and to calculate the average spectral efficiency, we run 1000 independent simulations and average the results to get the final figures. In the simulation results, we compare the performance of the proposed Alg. 1 with that obtained by the equal power allocation where the latter assumes the solution obtained in (41) because in (41), same power is allocated over each spatial channel and subcarrier at the energy and information source nodes.

B. Achievable Spectral Efficiency Performance

Fig. 3 plots the average spectral efficiency for different values of power P. The optimization by the proposed Alg. 1 achieves significant gain in the spectral efficiency compared to the equal power allocation approach. As expected, increasing the power budget increases the achievable spectral efficiency.

Fig. 4 plots the average spectral efficiency versus the self-loop path gain or SI, γ_{LI}. It is interesting to note that unlike in the non-EH based systems, where SI hurts the simultaneous signal transmission and reception, the SI in Fig. 4

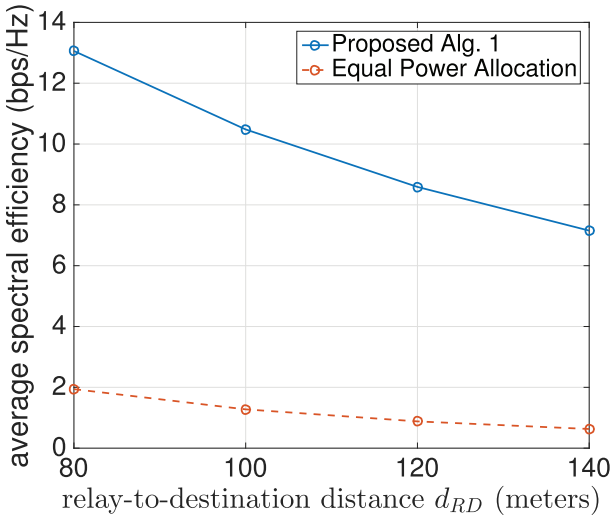

Fig. 5. Average spectral efficiency versus the relay-to-destination distance d_{RD}.

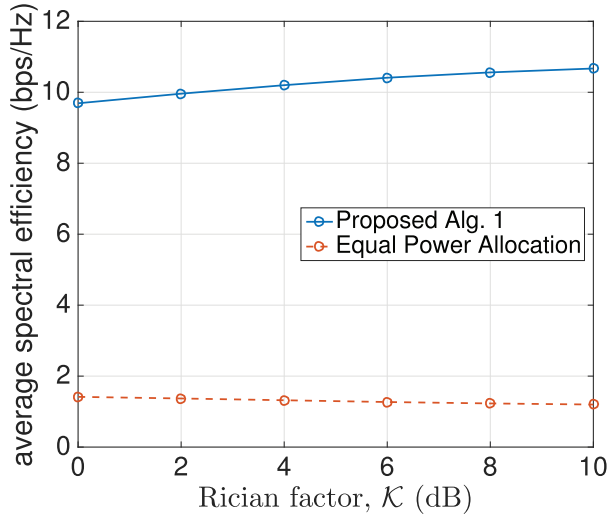

Fig. 6. Average spectral efficiency versus the Rician factor $\mathcal{K}$ of the time domain channel between energy source and relay.

enhances the achievable spectral efficiency. For example, it can be seen from Fig. 4 that the improvement in the spectral efficiency due to self-energy recycling is $\{0.14, 0.44\}$ bps/Hz at $\gamma_{LI} = \{-10, -6\}$ dB. Indeed, increase in the self-loop path gain results in more harvested energy from the loop SI, which is added to the available transmission power from R and that would improve the spectral efficiency at S. It is also clear from Fig. 4 that the optimization by the proposed Alg. 1 achieves significant gain in the spectral efficiency compared to the equal power allocation approach.

Fig. 5 plots the average spectral efficiency versus the relay-to-destination distance d_{RD}. As expected, the increase in the relay-to-destination distance decreases the achievable spectral efficiency due to increase in the path-loss. Fig. 6 plots the average spectral efficiency versus the Rician factor $\mathcal{K}$ of the time-domain channel $g_E^{n,\bar{n}}$. Fig. 6 shows that increase in the Rician factor results in increase in the achievable spectral efficiency of the proposed Alg. 1 only. The equal power allocation fails to show improvement in the spectral efficiency.

TABLE II
COMPUTATIONAL TIME OF PROPOSED ALG. 1 VERSUS (21) AND (23) BASED ITERATIONS

Solving Methodology	$K = 16$	$K = 64$	$K = 256$	$K = 1024$	$K = 4096$
Proposed. Alg. 1	0.01 sec	0.012 sec.	0.017 sec.	0.046 sec.	0.1602 sec.
(21) based iterations	8 mins	30 mins.	-	-	-
(23) based iterations	1.2 mins	3.1 mins	12.5	75 mins.	-

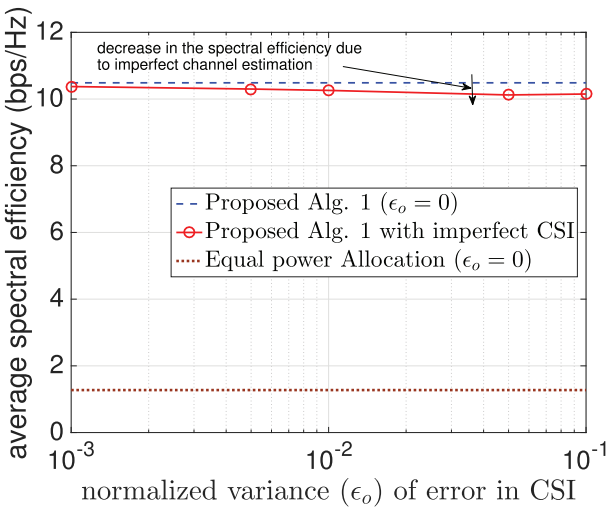

Fig. 7. Average spectral efficiency versus the normalized variance of channel estimation error.

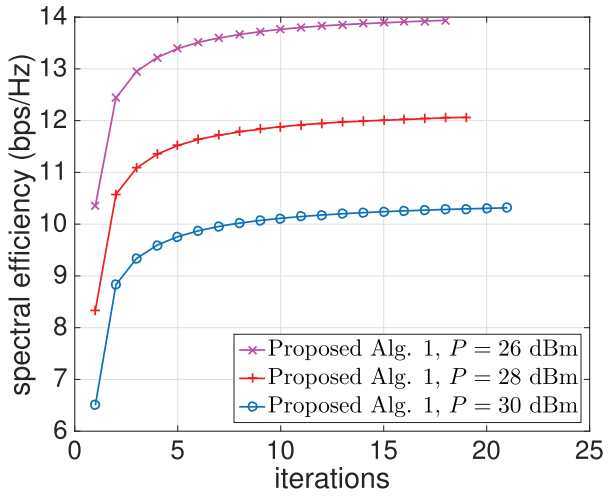

Fig. 8. The convergence of Proposed Alg. 1.

This is because though the E-to-R channel gets stronger by increasing its Rician factor which increases the R-to-D power under equal power allocation approach (see (41c)), such approach cannot guarantee an improved spectral efficiency as it allocates same power, no matter small or large, over all subcarriers of the R-to-D channel and thus, does not use the resources intelligently. It is also clear from Figs. 5-6 that the optimization by the proposed Alg. 1 achieves significant gain in the spectral efficiency compared to the equal power allocation approach. This significant gain is due to nature of the OFDM channel, where equal power allocation over all subcarriers suffers a lot compared to the optimal resource allocation.

Fig. 7 shows the impact of erroneous channel state information (CSI) on the achievable spectral efficiency. The results are plotted with respect to the normalized variance, ϵ_o, of the channel estimation error. By normalized variance, we mean that the variance is normalized with respect to the squared channel magnitude, e.g., if $\delta_{S,\ell}^{n,\bar{n}} = \left[\mathbf{g}_S^{n,\bar{n}}\right]_\ell - \left[\hat{\mathbf{g}}_S^{n,\bar{n}}\right]_\ell$ is the channel estimation error for the ℓ-th tap of the S-to-R channel and $\left[\hat{\mathbf{g}}_S^{n,\bar{n}}\right]_\ell$ is its estimate, then $\delta_{S,\ell}^{n,\bar{n}} \sim \mathcal{N}\left(0, \epsilon_o \left|\left[\mathbf{g}_S^{n,\bar{n}}\right]_\ell\right|^2\right)$. Similarly, the channel estimation error for the R-to-D channel, $\mathbf{g}_R^{n,\bar{n}}$, and the E-to-R channel, $g_E^{n,\bar{n}}$, subject to the same normalized variance ϵ_o. The results shows that the spectral efficiency is very mildly affected due to the erroneous channel estimation which shows the robustness of the proposed algorithm even in the presence of imperfect channel estimation.

C. Computational Complexity and Performance Comparison

Fig. 8 shows the convergence of the proposed Alg. 1 for different values of the power budget P for a particular simulation. We can see that the algorithm converges quickly after 20-25 iterations. On average, Alg. 1 requires $\{21.0, 19.46, 18.26, 17.14\}$ iterations before convergence for $P = \{26, 28, 30, 32\}$ dBm. Fig. 8 shows that the required number of iterations decreases with an increase in the power budget, which means that the Alg. 1 quickly figures out the optimal resource allocation in the presence of a relatively large power budget.

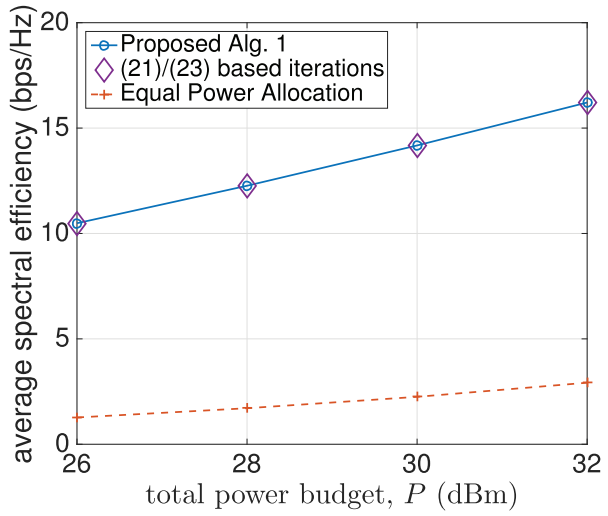

Fig. 9. Comparison of average spectral efficiency versus the total power budget P for different algorithms.

The closed-form solution proposed in Alg. 1 with the linear computational complexity (42), which is less than $(2KN + N)^3$ times compared with the polynomial computational complexity (24) for computing (23), is computationally

very efficient. The computational time of the proposed Alg. 1, which is calculated on a 2.7 GHz Intel core-i5 machine with 8 GB RAM, is shown in Table II for various system implementations (different numbers of subcarriers). In order to simulate small-scale system with $K = 16$ subcarriers or $K = 64$ subcarriers, we generate $\mathbf{g}_S^{n,\bar{n}}$ and $\mathbf{g}_R^{n,\bar{n}}$ with an exponential power delay profile having root-mean-square delay spread of $\sigma_{\text{RMS}} = T_s$, which results in $L = 4$-tap channel. Table II shows that the Alg. 1 quickly locates the optimal solution (in less than $\frac{1}{10}$ seconds). The computational time increases very slightly as the scale of the problem grows (as the number of subcarriers K increases). Note that the (23)-based or (21)-based iterations already consume a lot of time even for small-scale problems (with $K = 64$ or $K = 256$).

By Fig. 9, we compare the average spectral efficiency of Alg. 1 with that invoking (21) or (23). To ensure reasonable simulation time for solving (21) or (23) using CVX, we consider only a small-scale problem for $K = 64$. It can be seen from Fig. 9 that the proposed Alg. 1 achieves similar spectral efficiency performance as that obtained by invoking (21) or (23). However, Table II particularly indicates that the proposed Alg. 1 is almost $150,000$ or $15,500$ times computationally faster than that invoking (21) or (23), respectively.

V. Conclusion

This paper has considered a MIMO-OFDM based wireless-powered relaying communication, in which the cooperative relay forwards the source information to the destination while harvesting energy not only from wireless signals from a dedicated energy source but also through energy recycling from its own transmission. The high values of residual self-interference are helpful for wireless-powering the relay node. The objective is to maximize the spectral efficiency of such a system by power allocation over each subcarrier and each transmit antenna. This optimization problem, which is large scaled in the presence of a large number of subcarriers, is very computationally challenging. The paper has proposed a new path-following algorithm, which is practical for large-scale optimization as it requires only a few *closed-form* calculations of linear computational complexity. The provided simulations under practical assumptions show promising results by achieving high spectral efficiency, which is quite high compared to the simple "equal power allocation" approach.

Appendix: Basic Inequalities

As the function $\gamma(x) = \ln(1+x)$ is concave in the domain $\text{dom}(\gamma) = \{x > 0\}$, it is true that [44]

$$\begin{aligned}\ln(1+x) &\le \gamma(\bar{x}) + \frac{\partial \gamma(\bar{x})}{\partial x}(x-\bar{x}) \\ &= \ln(1+\bar{x}) + \frac{x-\bar{x}}{1+\bar{x}} \quad \forall\ x>0, \bar{x}>0. \end{aligned} \tag{43}$$

On the other hand, function $\beta(y) \triangleq \ln(1+e^y)$ is convex in the domain $\text{dom}(\beta) = \{y > 0\}$ because $\partial^2 f(y)/\partial y^2 = e^y/(1+e^y)^2 > 0\ \forall\ y \in \text{dom}(\beta)$. Therefore [44]

$$\begin{aligned}\ln(1+e^y) &\ge \beta(\bar{y}) + \frac{\partial \beta(\bar{y})}{\partial y}(y-\bar{y}) \\ &= \ln(1+e^{\bar{y}}) + \frac{e^{\bar{y}}}{1+e^{\bar{y}}}(y-\bar{y}). \end{aligned} \tag{44}$$

Substituting $x = e^y$ and $\bar{x} = e^{\bar{y}}$ into (44) yields the following inequality

$$\ln(1+x) \ge \ln(1+\bar{x}) + \frac{\bar{x}}{1+\bar{x}}\left(\ln x - \ln \bar{x}\right) \quad \forall\ x>0, \bar{x}>0. \tag{45}$$

References

[1] Z. Zhang, X. Chai, K. Long, A. V. Vasilakos, and L. Hanzo, "Full duplex techniques for 5G networks: Self-interference cancellation, protocol design, and relay selection," *IEEE Commun. Mag.*, vol. 53, no. 5, pp. 128–137, May 2015.

[2] B. K. Chalise, H. A. Suraweera, G. Zheng, and G. K. Karagiannidis, "Beamforming optimization for full-duplex wireless-powered MIMO systems," *IEEE Trans. Commun.*, vol. 65, no. 9, pp. 3750–3764, Sep. 2017.

[3] D. N. K. Jayakody, J. Thompson, S. Chatzinotas, and S. Durrani, Eds., *Wireless Information and Power Transfer: A New Paradigm for Green Communications*. New York, NY, USA: Springer, 2018.

[4] H. Hu, X. Da, L. Ni, Y. Huang, and H. Zhang, "Green energy powered cognitive sensor network with cooperative sensing," *IEEE Access*, vol. 7, pp. 17354–17364, 2019.

[5] J. Ren, J. Hu, D. Zhang, H. Guo, Y. Zhang, and X. Shen, "RF energy harvesting and transfer in cognitive radio sensor networks: Opportunities and challenges," *IEEE Commun. Mag.*, vol. 56, no. 1, pp. 104–110, Jan. 2018.

[6] D. Wang, R. Zhang, X. Cheng, and L. Yang, "Capacity-enhancing full-duplex relay networks based on power-splitting (PS-)SWIPT," *IEEE Trans. Veh. Technol.*, vol. 66, no. 6, pp. 5445–5450, Jun. 2017.

[7] L. Zhao, X. Wang, and T. Riihonen, "Transmission rate optimization of full-duplex relay systems powered by wireless energy transfer," *IEEE Trans. Wireless Comun.*, vol. 16, no. 10, pp. 6438–6450, Oct. 2017.

[8] Z. Wang, L. Li, H. Wang, and H. Tian, "Beamforming design in relay-based full-duplex MISO wireless powered communication networks," *IEEE Commun. Lett.*, vol. 20, no. 10, pp. 2047–2050, Oct. 2016.

[9] G. Chen, P. Xiao, J. R. Kelly, B. Li, and R. Tafazolli, "Full-duplex wireless-powered relay in two way cooperative networks," *IEEE Access*, vol. 5, pp. 1548–1558, 2017.

[10] W. Wang, R. Wang, W. Duan, R. Feng, and G. Zhang, "Optimal transceiver designs for wireless-powered full-duplex two-way relay networks with SWIPT," *IEEE Access*, vol. 5, pp. 22329–22343, 2017.

[11] X. Liu, Z. Wen, N. Du, C. Fan, and X. Tang, "Robust source-relay beamforming for full-duplex relay networks with energy harvesting," in *Proc. IEEE Globecom*, Dec. 2016, pp. 1–6.

[12] I. Orikumhi, C. Y. Leow, and Z. Ding, "Wireless information and power transfer in MIMO virtual full-duplex relaying system," *IEEE Trans. Veh. Technol.*, vol. 66, no. 12, pp. 11001–11010, Dec. 2017.

[13] A. A. Nasir, H. D. Tuan, D. T. Ngo, T. Q. Duong, and H. V. Poor, "Beamforming design for wireless information and power transfer systems: Receive power-splitting versus transmit time-switching," *IEEE Trans. Commun.*, vol. 65, no. 2, pp. 876–889, Feb. 2017.

[14] Z. Zhang, K. Long, A. V. Vasilakos, and L. Hanzo, "Full-duplex wireless communications: Challenges, solutions, and future research directions," *Proc. IEEE*, vol. 104, no. 7, pp. 1369–1409, Jul. 2016.

[15] H. D. Tuan, D. T. Ngo, and H. H. M. Tam, "Joint power allocation for MIMO-OFDM full-duplex relaying communications," *EURASIP J. Wireless Commun. Netw.*, vol. 2017, Jan. 2017, Art. no. 19, doi: 10.1186/s13638-016-0800-4.

[16] Z. Sheng, H. D. Tuan, T. Q. Duong, H. V. Poor, and Y. Fang, "Low-latency multiuser two-way wireless relaying for spectral and energy efficiencies," *IEEE Trans. Signal Process.*, vol. 66, no. 16, pp. 4362–4376, Aug. 2018.

[17] X. Lu, P. Wang, D. Niyato, D. I. Kim, and Z. Han, "Wireless networks with RF energy harvesting: A contemporary survey," *IEEE Commun. Surveys Tuts.*, vol. 17, no. 2, pp. 757–789, 2nd Quart., 2015.

[18] A. A. Nasir, X. Zhou, S. Durrani, and R. A. Kennedy, "Relaying protocols for wireless energy harvesting and information processing," *IEEE Trans. Wireless Commun.*, vol. 12, no. 7, pp. 3622–3636, Jul. 2013.
[19] Y. Zeng and R. Zhang, "Full-duplex wireless-powered relay with self-energy recycling," *IEEE Wireless Commun. Lett.*, vol. 4, no. 2, pp. 201–204, Apr. 2015.
[20] L. Zhang, Y. Cai, M. Zhao, B. Champagne, and L. Hanzo, "Nonlinear MIMO transceivers improve wireless-powered and self-interference-aided relaying," *IEEE Trans. Wireless Commun.*, vol. 16, no. 10, pp. 6953–6966, Oct. 2017.
[21] Z. Wei, X. Zhu, S. Sun, Y. Jiang, A. Al-Tahmeesschi, and M. Yue, "Research issues, challenges, and opportunities of wireless power transfer-aided full-duplex relay systems," *IEEE Access*, vol. 6, pp. 8870–8881, 2018.
[22] D. Hwang, S. S. Nam, and J. Yang, "Multi-antenna beamforming techniques in full-duplex and self-energy recycling systems: Opportunities and challenges," *IEEE Commun. Mag.*, vol. 55, no. 10, pp. 160–167, Oct. 2017.
[23] H. Kim, J. Kang, S. Jeong, K. E. Lee, and J. Kang, "Secure beamforming and self-energy recycling with full-duplex wireless-powered relay," in *Proc. IEEE Annu. Consum. Commun. Netw. Conf. (CCNC)*, Jan. 2016, pp. 662–667.
[24] M. Mohammadi, B. K. Chalise, H. A. Suraweera, C. Zhong, G. Zheng, and I. Krikidis, "Throughput analysis and optimization of wireless-powered multiple antenna full-duplex relay systems," *IEEE Trans. Commun.*, vol. 64, no. 4, pp. 1769–1785, Apr. 2016.
[25] A. Yadav, O. A. Dobre, and H. V. Poor, "Is self-interference in full-duplex communications a foe or a friend?" *IEEE Signal Process. Lett.*, vol. 25, no. 7, pp. 951–955, Jul. 2018.
[26] H. Liu, K. J. Kim, K. S. Kwak, and H. V. Poor, "Power splitting-based SWIPT with decode-and-forward full-duplex relaying," *IEEE Trans. Wireless Commun.*, vol. 15, no. 11, pp. 7561–7577, Nov. 2016.
[27] S. Hu, Z. Ding, and Q. Ni, "Beamforming optimisation in energy harvesting cooperative full-duplex networks with self-energy recycling protocol," *IET Commun.*, vol. 10, no. 7, pp. 848–853, May 2016.
[28] R. Chen and H. Zhang, "Power efficiency optimisation of wireless-powered full-duplex relay systems," *IET Commun.*, vol. 12, no. 5, pp. 603–611, Mar. 2018.
[29] Y. Su, L. Jiang, and C. He, "Decode-and-forward relaying with full-duplex wireless information and power transfer," *IET Commun.*, vol. 11, no. 13, pp. 2110–2115, Sep. 2017.
[30] W. Wu, B. Wang, Z. Deng, and H. Zhang, "Secure beamforming for full-duplex wireless powered communication systems with self-energy recycling," *IEEE Wireless Commun. Lett.*, vol. 6, no. 2, pp. 146–149, Apr. 2017.
[31] W. Wu, B. Wang, Y. Zeng, H. Zhang, Z. Yang, and Z. Deng, "Robust secure beamforming for wireless powered full-duplex systems with self-energy recycling," *IEEE Trans. Veh. Technol.*, vol. 66, no. 11, pp. 10055–10069, Nov. 2017.
[32] Q. N. Le, V. N. Q. Bao, and B. An, "Full-duplex distributed switch-and-stay energy harvesting selection relaying networks with imperfect CSI: Design and outage analysis," *J. Commun. Netw.*, vol. 20, no. 1, pp. 29–46, Feb. 2018.
[33] O. T. Demir and T. E. Tuncer, "Optimum QoS-aware beamformer design for full-duplex relay with self-energy recycling," *IEEE Wireless Commun. Lett.*, vol. 7, no. 1, pp. 122–125, Feb. 2018.
[34] A. Goldsmith, *Wireless Communications*. New York, NY, USA: Cambridge Univ. Press, 2005.
[35] Y. Cho, J. Kim, W. Y. Yang, and C. G. Kang, *MIMO-OFDM Wireless Communications With MATLAB*. Hoboken, NJ, USA: Wiley, 2010.
[36] I. Hammerstrom and A. Wittneben, "Power allocation schemes for amplify-and-forward MIMO-OFDM relay links," *IEEE Trans. Wireless Commun.*, vol. 6, no. 8, pp. 2798–2802, Aug. 2007.
[37] D. W. K. Ng and R. Schober, "Cross-layer scheduling for OFDMA amplify-and-forward relay networks," *IEEE Trans. Veh. Technol.*, vol. 59, no. 3, pp. 1443–1458, Mar. 2010.
[38] D. W. K. Ng, E. S. Lo, and R. Schober, "Dynamic resource allocation in MIMO-OFDMA systems with full-duplex and hybrid relaying," *IEEE Trans. Commun.*, vol. 60, no. 5, pp. 1291–1304, May 2012.
[39] S. Yin and Z. Qu, "Resource allocation in multiuser OFDM systems with wireless information and power transfer," *IEEE Commun. Lett.*, vol. 20, no. 3, pp. 594–597, Mar. 2016.
[40] X. Zhou, R. Zhang, and C. K. Ho, "Wireless information and power transfer in multiuser OFDM systems," *IEEE Trans. Wireless Commun.*, vol. 13, no. 4, pp. 2282–2294, Apr. 2014.
[41] D. W. K. Ng, E. S. Lo, and R. Schober, "Wireless information and power transfer: Energy efficiency optimization in OFDMA systems," *IEEE Trans. Wireless Commun.*, vol. 12, no. 12, pp. 6352–6370, Dec. 2013.
[42] K. Xiong, P. Fan, C. Zhang, and K. B. Letaief, "Wireless information and energy transfer for two-hop non-regenerative MIMO-OFDM relay networks," *IEEE J. Sel. Areas Commun.*, vol. 33, no. 8, pp. 1595–1611, Aug. 2015.
[43] K. Huang and X. Zhou, "Cutting the last wires for mobile communications by microwave power transfer," *IEEE Commun. Mag.*, vol. 53, no. 6, pp. 86–93, Jun. 2015.
[44] H. Tuy, *Convex Analysis and Global Optimization*, 2nd ed. Cham, Switzerland: Springer, 2017.
[45] H. H. Kha, H. D. Tuan, and H. H. Nguyen, "Fast global optimal power allocation in wireless networks by local D.C. programming," *IEEE Trans. Wireless Commun.*, vol. 11, no. 2, pp. 510–515, Feb. 2012.
[46] H. H. M. Tam, H. D. Tuan, D. T. Ngo, T. Q. Duong, and H. V. Poor, "Joint load balancing and interference management for small-cell heterogeneous networks with limited backhaul capacity," *IEEE Trans. Wireless Commun.*, vol. 16, no. 2, pp. 872–884, Feb. 2017.
[47] D. Peaucelle, D. Henrion, and Y. Labit. (2002). *Users Guide for SeDuMi Interface 1.03*. [Online]. Available: http://homepages.laas.fr/peaucell/software/sdmguide.pdf
[48] U. Rashid, H. D. Tuan, H. H. Kha, and H. H. Nguyen, "Joint optimization of source precoding and relay beamforming in wireless MIMO relay networks," *IEEE Trans. Commun.*, vol. 62, no. 2, pp. 488–499, Feb. 2014.
[49] H. H. M. Tam, H. D. Tuan, A. A. Nasir, T. Q. Duong, and H. V. Poor, "MIMO energy harvesting in full-duplex multi-user networks," *IEEE Trans. Wireless Commun.*, vol. 16, no. 5, pp. 3282–3297, May 2017.
[50] Y. Liu, Z. Qin, M. Elkashlan, A. Nallanathan, and J. A. McCann, "Non-orthogonal multiple access in large-scale heterogeneous networks," *IEEE J. Sel. Areas Commun.*, vol. 35, no. 12, pp. 2667–2680, Dec. 2017.
[51] A. Ghazanfari, H. Tabassum, and E. Hossain, "Ambient RF energy harvesting in ultra-dense small cell networks: Performance and trade-offs," *IEEE Wireless Commun.*, vol. 23, no. 2, pp. 38–45, Apr. 2016.

Ali Arshad Nasir (S'09–M'13) received the Ph.D. degree in telecommunications engineering from Australian National University (ANU), Australia, in 2013. He was a Research Fellow with ANU from 2012 to 2015. He held the position of an Assistant Professor with the School of Electrical Engineering and Computer Science (SEECS), National University of Sciences & Technology (NUST), Paksitan, from 2015 to 2016. He is currently an Assistant Professor with the Department of Electrical Engineering, King Fahd University of Petroleum and Minerals (KFUPM), Dhahran, KSA. His research interests are in the area of signal processing in wireless communication systems. He is also an Associate Editor of IEEE CANADIAN JOURNAL OF ELECTRICAL AND COMPUTER ENGINEERING.

Hoang Duong Tuan received the Diploma degree (Hons.) and the Ph.D. degree in applied mathematics from Odessa State University, Ukraine, in 1987 and 1991, respectively. He spent nine academic years in Japan as an Assistant Professor with the Department of Electronic-Mechanical Engineering, Nagoya University, from 1994 to 1999, and then, as an Associate Professor with the Department of Electrical and Computer Engineering, Toyota Technological Institute, Nagoya, from 1999 to 2003. He was a Professor with the School of Electrical Engineering and Telecommunications, University of New South Wales, from 2003 to 2011. He is currently a Professor with the School of Electrical and Data Engineering, University of Technology Sydney. He has been involved in research with the areas of optimization, control, signal processing, wireless communication, and biomedical engineering, for more than 20 years.

Trung Q. Duong (S'05–M'12–SM'13) received the Ph.D. degree in telecommunications systems from the Blekinge Institute of Technology (BTH), Sweden, in 2012.

He is currently with Queen's University Belfast, U.K., where he was a Lecturer (an Assistant Professor) from 2013 to 2017 and has been a Reader (an Associate Professor) since 2018. He is the author or coauthor of 290 technical articles published in scientific journals (165 articles) and presented at international conferences (125 articles). His current research interests include the Internet of Things (IoT), wireless communications, molecular communications, and signal processing. He also serves as an Editor for IEEE TRANSACTIONS ON WIRELESS COMMUNICATIONS, IEEE TRANSACTIONS ON COMMUNICATIONS, and *IET Communications,* and a Lead Senior Editor for IEEE COMMUNICATIONS LETTERS. He received the Best Paper Award at the IEEE Vehicular Technology Conference (VTC-Spring) in 2013, IEEE International Conference on Communications (ICC) 2014, IEEE Global Communications Conference (GLOBECOM) 2016, and IEEE Digital Signal Processing Conference (DSP) 2017. He is a recipient of the prestigious Royal Academy of Engineering Research Fellowship from 2016 to 2021 and has won the prestigious Newton Prize 2017.

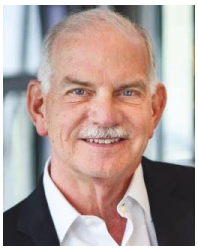

H. Vincent Poor (S'72–M'77–SM'82–F'87) received the Ph.D. degree in EECS from Princeton University in 1977.

From 1977 to 1990, he was on the faculty of the University of Illinois at Urbana–Champaign. Since 1990, he has been on the faculty at Princeton, where he is currently the Michael Henry Strater University Professor of Electrical Engineering. From 2006 to 2016, he served as the Dean of the Princeton's School of Engineering and Applied Science. He has also held visiting appointments at several other universities, including most recently at Berkeley and Cambridge. His research interests are in the areas of information theory and signal processing, and their applications in wireless networks, energy systems and related fields. Among his publications in these areas is the recent book *Multiple Access Techniques for 5G Wireless Networks and Beyond* (Springer, 2019).

Dr. Poor is a member of the National Academy of Engineering and the National Academy of Sciences, and also a Foreign Member of the Chinese Academy of Sciences, the Royal Society, and other national and international academies. He received the Marconi and Armstrong awards of the IEEE Communications Society in 2007 and 2009, respectively. Recent recognition of his work includes the 2017 IEEE Alexander Graham Bell Medal, the 2019 ASEE Benjamin Garver Lamme Award, the D.Sc. *honoris causa* from Syracuse University awarded in 2017, and the D.Eng. *honoris causa* from the University of Waterloo awarded in 2019.